Research Article | Vol. 32, No. 17 / 12 Aug 2024 / Optics Express 30114
Optics EXPRESS

Entanglement and classical nonseparability convertible from orthogonal polarizations

MINGHUI LI,[1] WEI WANG,[1] ZIKANG TANG,[1,†] AND HOU IAN[1,†,*]

[1] *Institute of Applied Physics and Materials Engineering, University of Macau, Macau S.A.R., China*
[†] co-last author
[*] *houian@um.edu.mo*

Abstract: The nonclassicality of a macroscopic single-mode optical superposition state is potentially convertible into entanglement, when the state is mixed with the vacuum on a beam splitter. Considering light beams with polarization degree of freedom in Euclidean space as coherent product states in a bipartite Hilbert space, we propose a method to convert the two orthogonal polarizations into simultaneous entanglement and classical nonseparability through nonclassicality in the superpositions of coherent and displaced Fock states. Equivalent Bell state emerges from the resulted superpositions and the proportion of mixed entanglement and nonseparablity is determined by the displacement amplitudes along the polarization directions. We characterize the state nonclassicality via features in Wigner distributions and propose an experimental method for generating these states and measuring them via homodyne tomography.

1. Introduction

At one end in the realm of optics, light of quantum nature is understood through the corpuscular concept of photon written as a Fock state. At the other end, its classical counterpart is embodied by a monochromatic beam written as a coherent state. The linkage between the two ends is the extension of finite-dimensional state space to infinite dimensions, in which the coherent state is equivalent to an infinite superposition of Fock states with Poisson distributed photon statistics [1]. Although the delineation between the classical regime and the quantum regime remains blurred, it is quite clear that the progression from the quantum state to the classical state of light is nuanced and a class of states belonging to neither extreme, known as nonclassical states of light [2–4], occupies the middle ground.

The inclusive term comprises a variety of states. Besides the familiar squeezed states and Schrödinger cat states, it also encompasses a genre of states connected to the nominally classical end: derivative states from coherent states. It includes the single-photon-added coherent state (SPACS, essentially $a^\dagger|\alpha\rangle$) [5,6], the displaced Fock state (DFS, $D(\alpha)|1\rangle$) [7,8], and superpositions of two coherent states ($|\alpha\rangle + |\beta\rangle$) [9]. The forementioned states have a quantifiable nonclassicality determined by entanglement potential [10,11], which measures the entanglement convertible from them when mixed with a vacuum state using just linear optical components and photodetectors. These investigations open up the possibility of quantum optical computation using macroscopic nonclassical states derived from classical light beams [12–15]. However, to what exact quantum state an arbitrarily polarized laser beam is mappable remains an open question. Specifically, from a quantitative perspective, it is still unclear how quantum and classical characteristics vary when two macroscopic orthogonal polarizations are converted into entangled states.

To these ends, we study entanglement as well as classical nonseparability [16–20] obtainable from a plane-wave electric field with two orthogonal polarizations. The latter has seen recent usages in coding quantum-like information by using structured light [21–25]. To retain the full gradation over the progression from the classical to the quantum regime, we consider the electric field that experiences several stages of splitting and recombining in a light path, where the only

#534088 https://doi.org/10.1364/OE.534088
Journal © 2024 Received 29 Jun 2024; revised 24 Jul 2024; accepted 24 Jul 2024; published 5 Aug 2024

Optics EXPRESS

quantum component is a quadrature operation realizable with parametric down conversion and projective detection. We show that the full range of entanglement and classical nonseparability can be obtained and co-exist with suitable polarizations in the two directions when converted. The convertibility demonstrates not only the potential [10] that entanglement would emerge from classical states, but also the overlap of classical nonseparability originating from two macroscopic field components. In addition, the converted light containing the polarization direction and the photon number degrees of freedom also enriches the studies of classical nonseparability in structured light [25].

Here, entanglement and classical nonseparability are treated in a unified Hilbert space for quantifying their convertibility from the macroscopic polarizations. Specifically, the x and y polarizations of an electric field vector in Euclidean space $\mathbb{R}^3$ are expressed as coherent states in the infinite dimensional Hilbert spaces $\mathcal{H}_x$ or $\mathcal{H}_y$ parametrized by continuous displacements. The entanglement and nonseparability then both emerge as measures on a superposition state $|\psi\rangle$ in the product space $\mathcal{H} = \mathcal{H}_x \otimes \mathcal{H}_y$. As quantifying metrics, their distinction is only mathematical: entanglement appears as a functional (we measure it in negativity [26]) directly on the Hilbert space vector $|\psi\rangle$ while nonseparability appears as a functional (we measure it in Schmidt number [17,18]) on the Euclidean space vector $\mathbf{E} = \langle\psi|\hat{E}|\psi\rangle$ derived from the field operator $\hat{E}$.

This unified approach assists in distinguishing the quantum entanglement and classical nonseparability within a single nonclassical state of light, according to the intuition to distinguish packetized photons expressed as Fock states from classical single-mode beams expressed as coherent states. For examples, as our discussions below will show, the apparent product state $|\psi\rangle = |\alpha\rangle_x \otimes |i\alpha\rangle_y$ has a maximal Schmidt number for classical nonseparability but zero negativity for entanglement. At the opposite extreme, the superposition $|1^{(\gamma)}\rangle_x|\delta\rangle_y + |\gamma\rangle_x|1^{(\delta)}\rangle_y$ of the orthogonal coherent states and DFSs, becoming the analogue of Bell states in the continuous space, obtains maximal negativity with vanishing Schmidt number. In these nonclassical states, the complex displacements α, γ, and δ derived from the polarization amplitudes serve as important indicators for the eventually convertible entanglement and classical nonseparability.

We give a detailed analysis of this convertibility when only one quantum operation is inserted along a linear optical path below. We remark that the choice of entanglement and classical nonseparability measures are independent of the results obtained. For example, if we use the Vogel-Sperling version of Schmidt number [27] that measures entanglement as a functional on $|\psi\rangle$, the obtained variation against the displacements would coincide with those obtained from the negativity. Wigner distributions representing the density matrix of the quantum states are used throughout to visualize the appearance of nonclassical states against the classical ones.

2. Generating entangled state

To substantiate the brief description above, we consider a gedanken experiment that produces any entangled state of varying degrees of negativity and Schmidt number, as shown in Fig. 1. A single-mode laser operating well above the threshold is considered the input source. It shows a coherent state excitation and thus exhibits an almost classical behavior [1]. Regarded as a plane wave carrying two independent polarizations, it has the joint state $|\psi_0\rangle = |\xi\rangle_x|\eta\rangle_y \in \mathcal{H}_x \otimes \mathcal{H}_y$ where x and y indicate a pair of orthogonal polarization directions. In other words, photons in $\mathcal{H}_x$ possess polarization opposite to those in $\mathcal{H}_y$ [28].

The laser beam is first split into two according to the polarization, after which the x-polarized part along path 1 undergoes a quadrature operation $q = a + a^\dagger$ while the y-polarization along path 2 is rotated by the HWP1 into x-polarization. The mathematical q-operation is optically implemented by parametric down conversion (PDC) with parametric gain g: the $|\xi\rangle_1$ beam serves as the signal while a beam with state $|0\rangle_i + g\xi|1\rangle_i$ serves as the idler input. At the output end, when the weak idler is measured by a photon detector and only single-photon events are selected, the signal output becomes conditioned and post-selected to the pure state $(a_1 + a_1^\dagger)\,|\xi\rangle_1$,

Optics EXPRESS

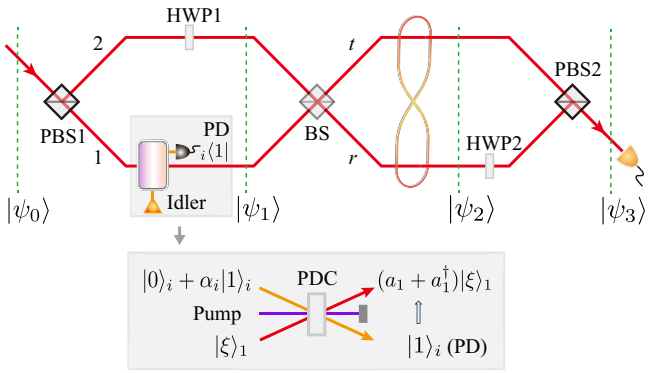

Fig. 1. Gedanken scheme for constructing a macroscopic entangled state: an initial product state $|\psi_0\rangle$ of a polarized beam goes through multiple stages to become entangled in the final state $|\psi_3\rangle$ before it is detected. First, $|\psi_0\rangle$ is split into two paths by a polarizing beam splitter (PBS1), after which one polarization branch (path 1) undergoes a conditional quadrature operation $q = a + a^\dagger$. Shown in the inset, this operation is implemented by a parametric down-conversion (PDC) followed by a photon detection (PD), forming a superposition of a coherent state and a SPACS. The other path 2 is rotated by a half-wave plate (HWP1) to interfere with path 1 through a balanced beam splitter (BS). The branched beams described by the product state $|\psi_1\rangle$ is thus mixed to generate the entangled state $|\psi_2\rangle$ that propagates along the transmission t and the reflection r directions after splitting. The r mode is rotated by HWP2 to align its polarization orthogonal to the t mode before they are recombined by PBS2 to form the final macroscopic entangled state $|\psi_3\rangle$.

a superposition of coherent and SPAC states [6,29]. The nonclassicality of this superposition state is crucial for generating quantum entanglement with a beam splitter [30], as we will see later.

At this stage, the system state is $|\psi_1\rangle = (a_1 + a_1^\dagger)\,|\xi\rangle_1\,|\eta\rangle_2\,/\sqrt{N}$ with N being the normalization constant, where we have used the path subscripts to differentiate the branched beams since both paths are now x-polarized. The two beams are combined by a 50-50 beam splitter (BS), which effectively perform the transformation $a_{1,2} \to (a_t \mp a_r)/\sqrt{2}$ on the annihilation operators as well as their Hermitian conjugates before and after the beam splitting [31]. That means, for instance, removing one photon in path 1 is equivalent to removing one photon either at the transmission beam or the reflection beam. Carrying out the algebraic operation on $|\psi_1\rangle$, the BS output is the state

$$|\psi_2\rangle = \frac{(q_t - q_r)}{\sqrt{2N}} \left|\frac{\eta+\xi}{\sqrt{2}}\right\rangle_t \left|\frac{\eta-\xi}{\sqrt{2}}\right\rangle_r \tag{1}$$

in the product space $\mathcal{H} = \mathcal{H}_t \otimes \mathcal{H}_r$ of the two branches. The state $|\psi_2\rangle$ is already an macroscopic entangled state with respect to the t and r beams, converted from the nonclassical state $|\psi_1\rangle$. The beam splitting effects the transformation $q_1 \to (q_t - q_r)/\sqrt{2}$ on the quadrature operator and the transformation $D_1(\xi)D_2(\eta) \to D_t((\eta+\xi)/\sqrt{2})D_r((\eta-\xi)/\sqrt{2})$ on the displacement operators (see Supplement 1 section 1 for derivation details). In the latter, the displacement amounts from the vacuum are essentially the polarizations in the macroscopic beam, i.e. the transmission and the reflection contains polarization originated from both path 1 and path 2. Therefore, measuring either the t- or the r-subspace would already yield information from both the original $\mathcal{H}_x$ and $\mathcal{H}_y$ spaces.

The quadrature difference operator $(q_t - q_r)$ in Eq. (1) has two effects: (i) each quadrature operator creates a nonclassical superposition within its respective Hilbert space, and (ii) the difference operation as a whole generates entanglement across the two Hilbert spaces. By (i), we

Optics EXPRESS

mean the quadrature operation in either $\mathcal{H}_t$ or $\mathcal{H}_r$ effectively generates the state

$$q\,|\alpha\rangle = \left(a + a^{\dagger}\right)|\alpha\rangle = 2\alpha_R|\alpha\rangle + |1^{(\alpha)}\rangle \tag{2}$$

from any coherent state $|\alpha\rangle$ [32] such that the resulting superposition comprises a displaced Fock state (DFS) $\left|1^{(\alpha)}\right\rangle = D(\alpha)\,|1\rangle$ and the original coherent state with coefficient $\alpha_R = \Re\{\alpha\}$. Since $\left\langle\alpha|1^{(\alpha)}\right\rangle = 0$, the two terms on the RHS, though not eigenstates of q, are orthogonal. The nonclassicality of such a superposition is exhibited, qualitatively, by its heralded addition of idler photons [15] and, quantitatively, by its unique photon-number variance measured by Mandel's parameter $Q = \left\langle\Delta(a^{\dagger}a)^2\right\rangle / \left\langle a^{\dagger}a\right\rangle \geq 0$ [5,33]. As shown in Fig. 2(a), Q vanishes for the Fock state $|1\rangle$ when $|\alpha| = 0$ and converges to unity for a coherent state with Poissonian distribution over the Fock basis. For the nonclassical states, however, they may exhibit either sub-Poissonian (Q<1) or super-Poissonian (Q>1) distributions, depending on the displacement phase φ as shown in Fig. 2(b). In such situations, the nonclassicality can be verified by the negativity of the Wigner function in the phase space corresponding to the squeezed or anti-squeezed photon-number variance.

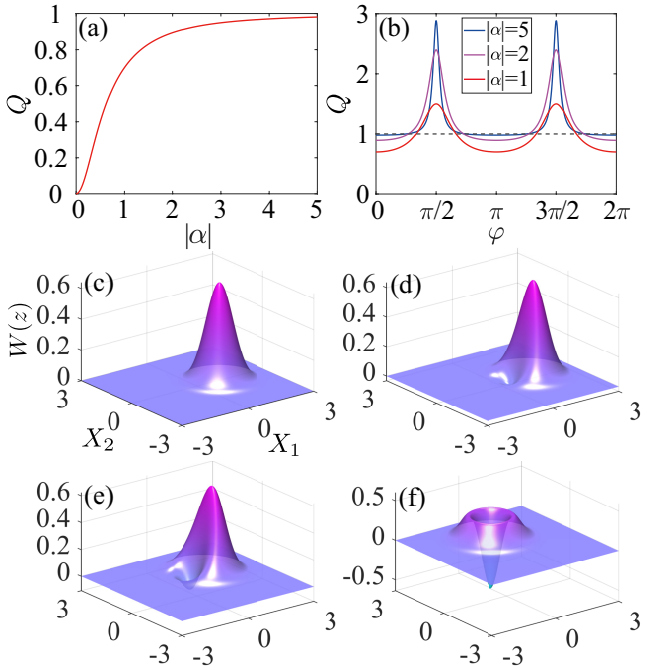

Fig. 2. Nonclassicality of a quadrature-operated coherent state, i.e. the superposition of a DFS and a coherent state, demonstrated through Q-parameter and Wigner distribution. Q-parameter as a function of (a) the displacement magnitude $|\alpha|$ when phase $\varphi = 0$ and (b) the displacement phase φ at various magnitudes. The superposition retains sub-Poissonian statistics for all $|\alpha|$ at zero phase but achieves super-Poissonian at $\pi/2$ and $3\pi/2$ phases. Accordingly, a varying squeezed state is formed, depending on the phase φ. Wigner distributions $W(z)$ over the phase space $z = X_1 + iX_2$ for (c) a coherent state with the Gaussian distribution and quadrature-operated coherent states with displacements (d) $\alpha = 1$, (e) $\alpha = (1 + i)/\sqrt{2}$, and (f) $\alpha = i$. The nonclassicality is characterized by negative values obtained in $W(z)$. Turning the displacement from the real to the imaginary axis, the distribution of negative W has increased until $|\psi\rangle$ reaches $\left|1^{(i)}\right\rangle$ that resembles most to a Fock state.

Optics EXPRESS

For instance, the nonclassicality of a SPACS can be characterized by a dipping towards negative axis in Wigner distributions [6]. For the nonclassical state of (2), its Wigner function being

$$W(z) = \frac{2}{\pi N}\left(4|z-\alpha_I|^2 - 1\right) e^{-2|z-\alpha|^2} \tag{3}$$

shows similar characterizations, as shown in Fig. 2(d)–(f). In the superposition of $|\alpha\rangle$ and $\left|1^{(\alpha)}\right\rangle$, the coherent-state term exemplifies when α has a large real part; whereas, only the DFS term remains when α is purely imaginary. Therefore, as shown in the plots, varying from $\alpha = 1$ to $\alpha = i$, the Wigner function is increasingly removed from the typical Gaussian for a coherent state towards a volcano-shaped surface with a center dip. This change coincides with the intuitive view of a classical-to-quantum crossover.

For effect (ii) of the difference operation over the nonclassical states generated from quadrature operations, we mean such operation would create entanglement between the photon statistics across the t- and the r-branch beams. To facilitate classical nonseparability on them, which is defined over a unified beam of orthogonal polarizations, the r-branch of the $|\psi_2\rangle$ is $\pi/2$-rotated by another half-wave plate (HWP2) and recombine with the t-branch using a polarizing beam splitter (PBS2). The resulting beam thus become x- and y-polarized again, whose quantum state reads

$$|\psi_3\rangle = \frac{1}{\sqrt{2N}}\left[\left|1^{(\mu_x)}\right\rangle|\mu_y\rangle - |\mu_x\rangle\left|1^{(\mu_y)}\right\rangle + 2\sqrt{2}\xi_R|\mu_x\rangle|\mu_y\rangle\right]. \tag{4}$$

Nevertheless, the displacements $\mu_x = (\eta+\xi)/\sqrt{2}$ and $\mu_y = (\eta-\xi)/\sqrt{2}$ differ largely from the original polarization magnitudes. Nonclassical superpositions with polarization-dependent coefficient $\xi_R = \Re\{\xi\}$ and the polarization remixing between ξ and η effects a state containing both quantifiable entanglement and classical nonseparability. Since the coherent states are orthogonal to both displaced Fock states in Eq. (4), $|\psi_3\rangle$ is akin to a Bell state in a two-qubit Hilbert space when ξ_R vanishes.

State $|\psi_3\rangle$ is an entangled state containing both the quantum entanglement and the classical nonseparability. The entanglement is measured by negativity [26] on a pure-state density matrix $\rho = |\psi\rangle\langle\psi|$ through a partial transpose T on one of the subspaces. We extend negativity to the continuous spaces to have $\mathcal{N}(\rho) = (||\rho^{T_x}||_1 - 1)/2$, where the partial transpose is applied on $\mathcal{H}_x$ and the trace norm $||\cdot||_1$ is effectively the finite sum of negative eigenvalues of ρ^{T_x} (see Supplement 1 section 2 for details), to find

$$\mathcal{N}(\rho) = \frac{1}{2+8\xi_R^2}. \tag{5}$$

When the displacement is purely imaginary along the vertical quadrature axis with $\xi_R = 0$, $\mathcal{N}(\rho)$ obtains its maximal value $1/2$, verifying our expectation that the case corresponds to a purely quantum Bell-like $|\psi_3\rangle$.

3. Mixture of entanglement and classical nonseparability

On the other hand, the classical nonseparability, measured by Schmidt number, has been defined through the electric field vector $\mathbf{E}$ in Euclidean space [18] rather than the density matrix since the classical picture lacks the Hilbert space description. To reconcile this conflict with the quantum interpretation, we promote the field vector to the field operator $\hat{E} = \hat{E}_x + \hat{E}_y$ over the two polarizations and compute Schmidt number from $\hat{E}$ as an observable on the last step of the gedanken experiment of Fig. 1 (indicated as a detector). Writing $\hat{E}_x = \mathbf{e}_x \mathscr{E} a_x \exp\{-i(\omega t - kz)\} + \text{h.c.}$ and similarly for $\hat{E}_y$ with field amplitude unit $\mathscr{E} = \sqrt{\hbar\omega/2\varepsilon_0 V}$ and polarization unit vector $\mathbf{e}_x$, the

Optics EXPRESS

measurement expectation of the field is

$$\mathbf{E} = \langle\psi_3|\hat{E}|\psi_3\rangle = \sum_{m\in\{x,y\}} \mathscr{E}\mathbf{e}_m \times [|\mu_m|\cos(\omega t - kz - \varphi_m) \pm r\cos(\omega t - kz)] \tag{6}$$

Here, φ_m denotes the phase of μ_m, $r = \sqrt{2}\xi_R/(1+4\xi_R^2) = \sqrt{2}\xi_R/N$ measures the horizontal displacements in the original coherent state $|\xi\rangle_x$, and the sign of the second term is + (−) for x- (y-) polarization (see Supplement 1 section 3 for details). The overlap of the polarization amplitudes into one another direction is obvious in Eq. (6), in addition to the extra r term which appears in y-polarization despite its origin in the x-polarization.

Such overlap constitutes a finite classical separability as reflected in the Schmidt number $K(\mathcal{W}) = \left[1 - \sin^2(\Delta\phi)\sin^2(2\theta)/2\right]^{-1}$ defined through a polarization matrix $\mathcal{W}$ in the lab frame [34]. The Schmidt number, falling in the range of $1 \le K \le 2$, represents the degree of classical nonseparability [17,18]. The lower bound corresponds to a separable state, while the upper bound indicates a Bell-like state. The mixture of polarization appears in both the new polarization angle

$$\theta = \arctan\sqrt{\frac{|\mu_y|^2 - 2r|\mu_y|\cos\varphi_y + r^2}{|\mu_x|^2 + 2r|\mu_x|\cos\varphi_x + r^2}} \tag{7}$$

and the difference $\Delta\phi = \phi_y - \phi_x$ between the new phases

$$\phi_m = \arctan\left(\frac{|\mu_m|\sin\varphi_m}{|\mu_m|\cos\varphi_m \pm r}\right), \tag{8}$$

the sign being + (−) for x-(y-) polarization. At $r = 0$, $K(\mathcal{W})$ obtains its maximal value when $\mu_y = \pm i\mu_x$, i.e. when $\xi_R = \eta_I$ and $\xi_I = \pm\eta_R$; the case where the y-polarization is $\pi/2$ ahead (behind) the x-polarization or the beam at $|\psi_0\rangle$ is CCW (CW) circularly polarized. If $r \neq 0$, one of the scenario for maximal $K(\mathcal{W})$ associates with the conditions $\mu_y = -\mu_x^*$, i.e. when $\xi_R/\xi_I = -\eta_I/\eta_R$. This case includes the previous scenario as a subset and other scenarios of disproportioned amplitudes among ξ and η, the latter of which correspond to beams with elliptical polarization.

Since the negativity depends on the polarization amplitude ξ_R while the Schmidt number depends on the scaled r, their extrema do not coincide but are obtainable independently despite the functional dependence of r on ξ_R. The entanglement and the classical nonseparability can be separately maximized or minimized depending on the input beam polarization, as shown in Table 1, where the only common constraint is $r = 0$. In particular, the simultaneity of maximal negativity (5) and Schmidt number occurs for a circularly polarized beam with zero ξ_R in its x-polarization. Conversely, a linearly polarized beam with proportional x- and y- polarizations such that $\xi_R = \eta_R$ is sufficiently large generates the simultaneous minimum. For the latter, the large ξ_R and η_R limit corresponds to vanishing μ_y and r, leading the $\mathbf{E}$ field of Eq. (6) back to a unmixed classical state containing only x-polarization.

Figures 3(a)–(b) show, respectively, negativity and Schmidt number as functions of ξ_R and η_I. Negativity is symmetric about the $\xi_R = 0$ axis. Since the quadrature q only measures x-polarized component along light path 1 in Fig. 1, it verifies that the quantum entanglement is solely associated with vacuum or displaced Fock states. Because of its asymmetric placement between paths 1 and 2, the quadrature operation further breaks the mirror symmetry about the $\xi_R = 0$ plane in the Schmidt number that measures the classical nonseparability. Rather, the mirror symmetry arises on the diagonal $\xi_R = \pm\eta_I$ planes when the operation on the state $|\psi_1\rangle$ has mitigated effects for large ξ_R and the two light paths have symmetric polarization magnitudes.

Optics EXPRESS

Table 1. Conditions among the beam *x*- and *y*-polarizations $\xi = \xi_R + i\xi_I$ and $\eta = \eta_R + i\eta_I$ for obtaining the extrema of the negativity $\mathcal{N}(\rho)$ and the Schmidt number $K(\mathcal{W})$, where r is set to zero. k is a real proportional constant.

	$\mathcal{N}(\rho)$ max	$\mathcal{N}(\rho)$ min
$K(\mathcal{W})$ max	$\xi_R = \eta_I = 0$ $\xi_I = \pm\eta_R$	$\xi_R \to \infty$ $\eta = \pm i\xi$
$K(\mathcal{W})$ min	$\xi_R = \eta_R = 0$ $\xi_I = \pm k\eta_I$	$\xi_R \to \infty$ $\eta = \pm k\xi$

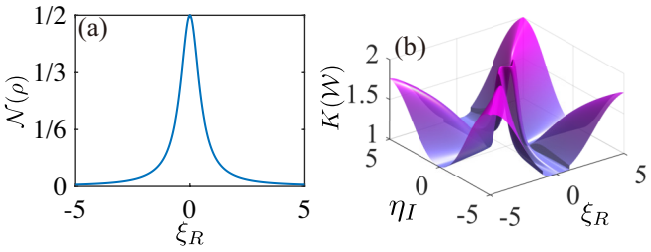

Fig. 3. (a) Negativity for measuring the quantum entanglement and (b) Schmidt number for measuring the classical nonseparability. Both measures the nonclassical state $|\psi_3\rangle$, and for (b) $\eta_R = 1$ and $\xi_I = -1$.

4. Experimental proposal for state detection

As illustrated in Fig. 2 above, the nonclassical superposition state $|\psi_2\rangle$ is uniquely described by a Wigner distribution $W(z)$ [6,7,35]. The entangled $|\psi_3\rangle$ containing a mixture of entanglement and classical nonseparability over the Hilbert spaces $\mathcal{H}_x$ and $\mathcal{H}_y$ can then be detected using Wigner distributions along both polarization directions. The measured results correspond to the parameters of the generated states, indicating the structures of light across different degrees of freedom. The character of the mixture is readily identified by the unique locations and shapes derived from tomographic measurement on either polarization, where the other polarization is traced out over the orthogonal basis $\{|\mu_m\rangle, |1^{(\mu_m)}\rangle\}$. For instance, if we measure the density matrix $\rho_x = \mathrm{tr}_y\{|\psi_3\rangle\langle\psi_3|\}$ on the x-polarization, its Wigner distribution reads

$$W(z) = \frac{4|z - \mu_x + \sqrt{2}\xi_R|^2}{(1 + 4\xi_R^2)\pi} e^{-2|z-\mu_x|^2}, \tag{9}$$

for which the circular symmetry about $z = \mu_x$ is broken by the addition of $\sqrt{2}\xi_R$ in the quadratic factor but not in the Gaussian, echoing the effect we already observed in Fig. 3(b). Geometrically, the symmetry breaking corresponds to a transition from a volcano shape to one with a slanted crest, as shown in Fig. 4(a)–(b).

Removed from the origin, the relative locations of the displacement of μ_x and μ_y on the quadrature plane determine the degrees of both entanglement and classical nonseparability convertible from $|\mu_x\rangle|\mu_y\rangle$. For instance, as shown in Fig. 4(c)–(e), the case of simultaneous maximal entanglement and classical nonseparability occurs for μ_x and μ_y symmetric about the horizontal quadrature axis, i.e. they having the same real part but non-zero opposite imaginary parts. When the imaginary part vanishes and hence the displacements coincide, only the entanglement survives. All states with coinciding displacements are purely entangled states (without classical nonseparability) though this is not true vice versa as inferred from Eqs. (7)–(8).

Optics EXPRESS

When the displacements become large and differ by a phase of $\pi/2$, the classical nonseparability survives and the entanglement vanishes.

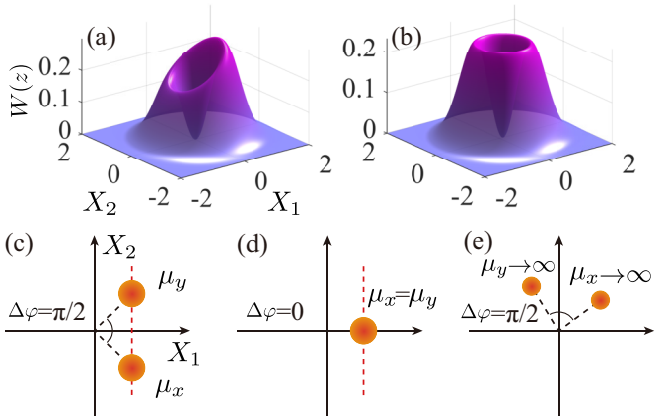

Fig. 4. Wigner distributions about the reduced density matrix ρ_x (associated with x-polarization of the output light beam at state $|\psi_3\rangle$). Surface plots for small displacements $\mu_x = (\xi + \eta)/\sqrt{2} = 0.1$ are shown in (a) where $\sqrt{2}\xi_R = 0.1$ and in (b) where $\sqrt{2}\xi_R = 0$. The slight difference in ξ_R incurs a symmetry breaking about the center. Contour plots for large displacements are shown in (c)–(e): (c) shows the case where entanglement and classical nonseparability are both maximal; (d) shows the case with maximal entanglement and vanishing classical nonseparability; and (e) shows the case with maximal classical nonseparability and vanishing entanglement.

To demonstrate the varying degrees of entanglement and classical nonseparability, we consider the experimental setup shown in Fig. 5. The single-mode light source is generated from a picosecond pulsed mode-locked laser, which is split into two paths by a BS: one is used as the local oscillator (LO) input for the homodyne detection later on and the other is further split into three paths. The pulses along the first path is attenuated by a variable filter (VF) to act as the weak idler $|\alpha_i\rangle_x \approx |0\rangle_x + \alpha_i|1\rangle_x$. The second path is fed to a nonlinear crystal for second harmonic generation (SHG), generating the pump pulses for the PDC. The third path goes through a fiber polarization controller (FPC) to generate an arbitrarily polarized initial state $|\psi_0\rangle$. Through the subsequent polarizing beam splitter, $|\psi_0\rangle$ is split into the two orthogonally polarized states $|\xi\rangle_x$ and $|\eta\rangle_y$. The half-wave plate HWP1 rotates $|\eta\rangle_y$ into $|\eta\rangle_x$ such that the two polarizing paths interfere with each other at BS1.

Before the interference at BS1, $|\xi\rangle_x$ acting as the signal is mixed with the idler $|\alpha_i\rangle_x$ and the pump at a nonlinear crystal for the PDC process. For simplicity, we omit the polarization subscript and denote the input signal and idler by the product state $|\xi\rangle_1 (|0\rangle_i + \alpha_i|1\rangle_i)$. The quadrature operation in Fig. 1 is conditioned on single-photon measurements of the idler output at PD after the three-wave mixing. The mixing approximately has the effect of $1 + g a_1^\dagger a_i^\dagger + g^* a_1 a_i$ on the input state $|\xi\rangle_1 (|0\rangle_i + \alpha_i|1\rangle_i)$ when the parametric gain g is sufficiently low ($|g| \ll 1$) [6], giving the output

$$(1 + g^*\xi\alpha_i)\,|\xi\rangle_1\,|0\rangle_i + (\alpha_i + g a_1^\dagger)\,|\xi\rangle_1\,|1\rangle_i + \sqrt{2} g\alpha_i a_1^\dagger\,|\xi\rangle_1\,|2\rangle_i. \tag{10}$$

When one photon is recorded by the PD, the signal state is projected onto $g(\alpha_i/g + a_1^\dagger)|\xi\rangle_1$. Letting $\alpha_i = g\xi$, the emitted signal state would be equivalent to the desired $g(a_1 + a_1^\dagger)|\xi\rangle_1$ and the normalized system state would become $|\psi_1\rangle$.

The 50-50 beam splitting at BS1 then generates $|\psi_2\rangle$ as in Fig. 1 along two legs, which are spatially recombined by PBS2 after the reflection leg is rotated by HWP2. Hence, the final state

Optics EXPRESS

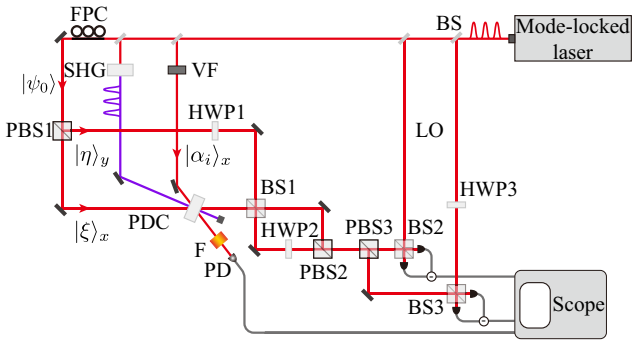

Fig. 5. Proposed experimental setup for detecting entangled and classically nonseparable states converted from nonclassical states. The components used include: beam splitters (BS), polarized beam splitters (PBS), half-wave plates (HWP), variable filters (VF), parametric down converter (PDC), second harmonic generator (SHG), and photon detectors (PD).

$|\psi_3\rangle$ containing complex amplitudes along both the x- and y-polarizations is prepared. The beam splittings at BS2 and BS3 separate the quadratures for each polarization direction, which are individually detected for their time correlations. The relative phase between the LO and the signal can be adjusted by a piezoelectric transducer (not shown) in the LO. The measurement results of PD after spectral and spatial filters (F), which herald the preparation of the nonclassical state, are used to select the results from balanced homodyne detection.

5. Conclusions and discussions

We demonstrate the convertibility of a classical polarized beam to an macroscopic entangled state, where the relationship between the degrees of quantum entanglement and classical nonseparability obtained from the polarizations of the beam is established. The convertibility is realized by the nonclassicality obtainable from a coherent single-mode beam through linear optics and, by inserting a quadrature operation asymmetrically along one polarization path, arbitrary mixtures of entanglement and classical nonseparability are eventually converted from an appropriate pair of displacements from the beam polarizations.

In other words, we have shown full range of quantum entanglement and classical nonseparability can be simultaneously generated from macroscopic polarizations. The generation method advances the study of controlling continuous variable quantum information and manipulation of different degrees of freedom in structured light. The computation method provides a means to characterize both the quantum and classical aspects of a single light state. The convertibility from polarizations here is useful for developing state preparation and quantum information processing techniques that take advantage of both the unique property of entanglement and the ease of operation of classical beams. Our proposed experimental setup demonstrates its viability.

Funding. Fundo para o Desenvolvimento das Ciências e da Tecnologia (006/2022/ALC, 0179/2023/RIA3).

Disclosures. The authors declare no conflicts of interest.

Data availability. Data underlying the results presented in this paper are not publicly available at this time but may be obtained from the authors upon reasonable request.

Supplemental document. See Supplement 1 for supporting content.

References

1. R. Loudon, *The Quantum Theory of Light* (Oxford University Press, 2000).
2. W. Vogel, "Nonclassical States: An Observable Criterion," Phys. Rev. Lett. **84**(9), 1849–1852 (2000).
3. C. T. Lee, "Measure of the nonclassicality of nonclassical states," Phys. Rev. A **44**(5), R2775–R2778 (1991).
4. V. V. Dodonov and V. I. Man'ko, *Theory of Nonclassical States of Light* (CRC, 2003).

Optics EXPRESS

5. G. S. Agarwal and K. Tara, "Nonclassical properties of states generated by the excitations on a coherent state," Phys. Rev. A **43**(1), 492–497 (1991).
6. A. Zavatta, S. Viciani, and M. Bellini, "Quantum-to-Classical Transition with Single-Photon-Added Coherent States of Light," Science **306**(5696), 660–662 (2004).
7. A. I. Lvovsky and S. A. Babichev, "Synthesis and tomographic characterization of the displaced Fock state of light," Phys. Rev. A **66**(1), 011801 (2002).
8. To simplify and unify the notations, we use $|\alpha^{(n)}\rangle$ to denote photon-added coherent states (a.k.a. Agarwal states) and $|n^{(\alpha)}\rangle$ to denote displaced Fock states throughout the paper.
9. W. Schleich, M. Pernigo, and F. L. Kien, "Nonclassical State from Two Pseudoclassical States," Phys. Rev. A **44**(3), 2172–2187 (1991).
10. J. K. Asbóth, J. Calsamiglia, and H. Ritsch, "Computable Measure of Nonclassicality for Light," Phys. Rev. Lett. **94**(17), 173602 (2005).
11. N. Killoran, F. E. S. Steinhoff, and M. B. Plenio, "Converting Nonclassicality into Entanglement," Phys. Rev. Lett. **116**(8), 080402 (2016).
12. N. Bruno, A. Martin, P. Sekatski, *et al.*, "Displacement of entanglement back and forth between the micro and macro domains," Nat. Phys. **9**(9), 545–548 (2013).
13. A. I. Lvovsky, R. Ghobadi, A. Chandra, *et al.*, "Observation of micro–macro entanglement of light," Nat. Phys. **9**(9), 541–544 (2013).
14. D. V. Sychev, V. A. Novikov, K. K. Pirov, *et al.*, "Entanglement of macroscopically distinct states of light," Optica **6**(11), 1425–1430 (2019).
15. N. Biagi, L. S. Costanzo, M. Bellini, *et al.*, "Entangling Macroscopic Light States by Delocalized Photon Addition," Phys. Rev. Lett. **124**(3), 033604 (2020).
16. R. J. C. Spreeuw, "A Classical Analogy of Entanglement. Foundations of Physics," Found. Phys. **28**(3), 361–374 (1998).
17. C. Gabriel, A. Aiello, W. Zhong, *et al.*, "Entangling Different Degrees of Freedom by Quadrature Squeezing Cylindrically Polarized Modes," Phys. Rev. Lett. **106**(6), 060502 (2011).
18. X.-F. Qian and J. H. Eberly, "Entanglement and classical polarization states," Opt. Lett. **36**(20), 4110 (2011).
19. E. Karimi and R. W. Boyd, "Classical entanglement?" Science **350**(6265), 1172–1173 (2015).
20. S. M. Hashemi Rafsanjani, M. Mirhosseini, O. S. Magaña-Loaiza, *et al.*, "State transfer based on classical nonseparability," Phys. Rev. A **92**(2), 023827 (2015).
21. G. Milione, T. A. Nguyen, J. Leach, *et al.*, "Using the nonseparability of vector beams to encode information for optical communication," Opt. Lett. **40**(21), 4887–4890 (2015).
22. D. Pierangeli, A. Aiello, and C. Conti, "Measuring the Tensorial Flow of Mosaic Vector Beams in Disordered Media," Phys. Rev. Lett. **132**(24), 243801 (2024).
23. Y. Shen and C. Rosales-Guzmán, "Nonseparable States of Light: From Quantum to Classical," Laser Photonics Rev. **16**(7), 2100533 (2022).
24. Z. Qing, W. Yan, X. Long, *et al.*, "Longitudinal manipulation of local nonseparability in vector beams," Opt. Lett. **49**(10), 2557–2560 (2024).
25. A. Forbes, M. de Oliveira, and M. R. Dennis, "Structured light," Nat. Photonics **15**(4), 253–262 (2021).
26. G. Vidal and R. F. Werner, "Computable measure of entanglement," Phys. Rev. A **65**(3), 032314 (2002).
27. W. Vogel and J. Sperling, "Unified Quantification of Nonclassicality and Entanglement," Phys. Rev. A **89**(5), 052302 (2014).
28. J. M. Jauch and F. Rohrlich, *The Theory of Photons and Electrons*, Sec. 2–8 (Springer, 1976).
29. K. J. Resch, J. S. Lundeen, and A. M. Steinberg, "Quantum State Preparation and Conditional Coherence," Phys. Rev. Lett. **88**(11), 113601 (2002).
30. M. S. Kim, W. Son, V. Bužek, *et al.*, "Entanglement by a beam splitter: Nonclassicality as a prerequisite for entanglement," Phys. Rev. A **65**(3), 032323 (2002).
31. S. Prasad, M. O. Scully, and W. Martienssen, "A quantum description of the beam splitter," Opt. Commun. **62**(3), 139–145 (1987).
32. K. P. Seshadreesan, J. P. Olson, K. R. Motes, *et al.*, "Boson sampling with displaced single-photon Fock states versus single-photon-added coherent states: The quantum-classical divide and computational-complexity transitions in linear optics," Phys. Rev. A **91**(2), 022334 (2015).
33. L. Mandel and E. Wolf, *Optical Coherence and Quantum Optics* (Cambridge University Press, 1995).
34. Z. You, Y. Wang, Z. Tang, *et al.*, "Measurement of classical entanglement using interference fringes," J. Opt. Soc. Am. B **38**(6), 1798 (2021).
35. G. Breitenbach, S. Schiller, and J. Mlynek, "Measurement of the quantum states of squeezed light," Nature **387**(6632), 471–475 (1997).